Broadband spoof plasmons and subwavelength electromagnetic energy confinement on ultrathin metafilms

Miguel Navarro-Cía,[1,2,*] Miguel Beruete,[1] Spyros Agrafiotis,[2] Francisco Falcone,[1] Mario Sorolla,[1] and Stefan A. Maier[2]

[1]*Millimeter and Terahertz Waves Laboratory, Universidad Pública de Navarra, Campus Arrosadía, 31006 Pamplona, Spain*

[2]*Experimental Solid State Group, Physics Department, Imperial College London, London SW7 2AZ, UK*

**miguel.navarro@unavarra.es*

Abstract: A complementary split ring resonator (CSRR)-based metallic layer is proposed as a route to mimic surface plasmon polaritons. A numerical analysis of the textured surface is carried out and compared to previous prominent topologies such as metal mesh, slit array, hole array, and Sievenpiper mushroom surfaces, which are studied as well from a transmission line perspective. These well-documented geometries suffer from a narrowband response, alongside, in most cases, metal thickness constraint (usually of the order of λ/4) and non-subwavelength modal size as a result of the large dimensions of the unit cell (one dimensions is at least of the order of λ/2). All of these limitations are overcome by the proposed CSRR-based surface. Besides, a planar waveguide is proposed as a proof of the potential of this CSRR-based metallic layer for spoof surface plasmon polariton guiding. Fundamental aspects aside, the structure under study is easy to manufacture by simple PCB techniques and it is expected to provide good performance within the frequency band from GHz to THz.

OCIS codes: (050.2065) Effective medium theory; (050.6624) Subwavelength structures; (160.1245) Artificially engineered materials; (160.3918) Metamaterials; (240.6680) Surface plasmons; (240.6690) Surface waves.

References and links

1. S. A. Maier, *Plasmonics: Fundamentals and Applications* (Springer, New York, 2007)
2. S. A. Maier, "Plasmonics: Metal nanostructures for subwavelength photonic devices," IEEE J. Sel. Top. Quantum Electron. **12**(6), 1214–1220 (2006).
3. J. B. Pendry, L. Martín-Moreno, and F. J. García-Vidal, "Mimicking surface plasmons with structured surfaces," Science **305**(5685), 847–848 (2004).
4. G. Goubau, "Surface waves and their application to transmission lines," J. Appl. Phys. **21**(11), 1119–1128 (1950).
5. F. J. García-Vidal, L. Martín-Moreno, and J. B. Pendry, "Surfaces with holes in them: new plasmonic metamaterials," J. Opt. A, Pure Appl. Opt. **7**(2), S97–S101 (2005).
6. S. A. Maier, S. R. Andrews, L. Martín-Moreno, and F. J. García-Vidal, "Terahertz Surface Plasmon-Polariton Propagation and Focusing on Periodically Corrugated Metal Wires," Phys. Rev. Lett. **97**, 1–4 (2006).
7. A. I. Fernández-Domínguez, C. R. Williams, F. J. García-Vidal, L. Martín-Moreno, S. R. Andrews, and S. A. Maier, "Terahertz surface plasmon polaritons on a helically grooved wire," Appl. Phys. Lett. **93**, 1–3 (2008).
8. M. J. Lockyear, A. P. Hibbins, and J. R. Sambles, "Microwave Surface-Plasmon-Like Modes on Thin Metamaterials," Phys. Rev. Lett. **102**, 1–4 (2009).
9. D. Sievenpiper, L. Zhang, R. F. Jimenez Broas, N. G. Alexópolous, and E. Yablonovitch, "High-Impedance Electromagnetic Surfaces with a Forbidden Frequency Band," IEEE Trans. Microw. Theory Tech. **47**(11), 2059–2074 (1999).
10. R. Marqués, F. Martín, and M. Sorolla, *Metamaterials with Negative Parameters: Theory, Design, and Microwave Applications* (John Wiley & Sons, New York, 2008).
11. L. Solymar, and E. Shamonina, *Waves in Metamaterials* (Oxford University Press, New York, 2009).
12. J. B. Pendry, A. J. Holden, D. J. Robbins, and W. J. Stewart, "Magnetism from conductors and enhanced nonlinear phenomena," IEEE Trans. Microw. Theory Tech. **47**(11), 2075–2084 (1999).
13. F. Falcone, T. Lopetegi, M. A. G. Laso, J. D. Baena, J. Bonache, M. Beruete, R. Marqués, F. Martín, and M. Sorolla, "Babinet principle applied to metasurface and metamaterial design," Phys. Rev. Lett. **93**, 1–4 (2004).

#115697 - $15.00 USD Received 13 Aug 2009; revised 11 Sep 2009; accepted 12 Sep 2009; published 24 Sep 2009

14. A. K. Sarychev, G. Shvets, and V. M. Shalaev, "Magnetic plasmon resonance," Phys. Rev. E Stat. Nonlin. Soft Matter Phys. **73**, 1–10 (2006).
15. H. Liu, D. A. Genov, D. M. Wu, Y. M. Liu, J. M. Steele, C. Sun, S. N. Zhu, and X. Zhang, "Magnetic Plasmon Propagation Along a Chain of Connected Subwavelength Resonators at Infrared Frequencies," Phys. Rev. Lett. **97**, 1–4 (2006).
16. M. Beruete, F. Falcone, M. J. Freire, R. Marqués, and J. D. Baena, "Electroinductive Waves in Chains of Complementary Metamaterial Elements," Appl. Phys. Lett. **88**, 1–3 (2006).
17. N. Liu, S. Kaiser, and H. Giessen, "Magnetoinductive and Electroinductive Coupling in Plasmonic Metamaterial Molecules," Adv. Mater. **20**(23), 4521 (2008).
18. R. Ulrich, and M. Tacke, "Submillimeter waveguide on periodic metal structure," Appl. Phys. Lett. **22**(5), 251–253 (1973).
19. R. Ulrich, "Modes of propagation on an open periodic waveguide for the far infrared," in Proceedings Symp. Opt. Acoust. Microelectron., (Polytechnic Press of the Polytechnic Institute of New York. New York, 1974).
20. C. R. Williams, S. R. Andrews, S. A. Maier, A. I. Fernández-Domínguez, L. Martín-Moreno, and F. J. García-Vidal, "Highly confined guiding of terahertz surface plasmon polaritons on structured metal surfaces," Nat. Photonics **2**(3), 175–179 (2008).
21. A. P. Hibbins, B. R. Evans, and J. R. Sambles, "Experimental Verification of Designer Surface Plasmons," Science **308**(5722), 670–672 (2005).
22. W. Zhu, A. Agrawal, and A. Nahata, "Planar plasmonic terahertz guided-wave devices," Opt. Express **16**(9), 6216–6226 (2008).
23. E. Hendry, A. P. Hibbins, and J. R. Sambles, "Importance of diffraction in determining the dispersion of designer surface plasmons," Phys. Rev. B **78**, 1–10 (2008).
24. D. Pozar, *Microwave Engineering* (John Wiley & Sons, New York, 2004).
25. G. V. Eleftheriades, and K. G. Balmain, *Negative-Refraction Metamaterials* (John Wiley & Sons, Hoboken, New Jersey, 2005).
26. C. Caloz, and T. Itoh, *Electromagnetic metamaterials: transmission line theory and microwave applications* (John Wiley & Sons, Hoboken, New Jersey, 2006).
27. R. Ulrich, "Far-infrared properties of metallic mesh and its complementary structure," Infrared Phys. **7**(1), 37–55 (1967).
28. M. Beruete, M. Aznabet, M. Navarro-Cía, O. El Mrabet, F. Falcone, N. Aknin, M. Essaaidi, and M. Sorolla, "Electroinductive waves role in left-handed stacked complementary split rings resonators," Opt. Express **17**(3), 1274–1281 (2009).
29. S. A. Maier, P. G. Kik, H. A. Atwater, S. Meltzer, E. Harel, B. E. Koel, and A. A. Requicha, "Local detection of electromagnetic energy transport below the diffraction limit in metal nanoparticle plasmon waveguides," Nat. Mater. **2**(4), 229–232 (2003).
30. X. Chen, T. M. Grzegorczyk, B. I. Wu, J. Pacheco, Jr., and J. A. Kong, "Robust method to retrieve the constitutive effective parameters of metamaterials," Phys. Rev. E Stat. Nonlin. Soft Matter Phys. **70**, 1–7 (2004).

1. Introduction

At optical frequencies, metals support fascinating optical interactions under p-polarization such as surface plasmons polaritons (SPPs) because the dielectric constant of metals in the visible and near-IR regions is predominantly real and negative. Among others characteristics, SPPs are bound surface states, with excess of in-plane momentum with respect to light of the same frequency, leading to an ever-increasing out-of-plane confinement as the surface plasmon frequency is approached. Thus, they are a powerful candidate for tightly bound planar waveguiding and this has been one of the major driving forces in plasmonics [1, 2].

At lower frequencies, i.e. microwaves and terahertz, or even under the limit of a perfect electric conductor (PEC), the properties of confined SPPs can be mimicked by geometrical induced SPPs, also known as spoof SPPs [3]. Geometrical tuning of the electromagnetic surface response overcomes the physical limitations imposed by the permittivity of metals at such frequencies, which is primarily imaginary. Thus, metals become very conducting and reflecting. In this scenario, SPPs on flat surfaces become Sommerfeld-Zenneck waves [4] which are loosely bound surface waves and whose delocalization hinders their application for planar guiding.

In their infancy, spoof SPPs were described on a one-dimensional array of grooves [5] and two-dimensional hole arrays [3] with subwavelength pitch. It was shown that their effective dielectric function resembles a Drude model, whose plasma frequency can be engineered via the geometry of the corrugations alone, allowing the inducing of SPPs-like states in any region of the spectrum where the PEC condition approximates the metallic response. Extensions to cylindrical geometries have been proposed and demonstrated [6, 7]. The spoof

#115697 - $15.00 USD Received 13 Aug 2009; revised 11 Sep 2009; accepted 12 Sep 2009; published 24 Sep 2009

SPP concept has recently also been analyzed using a *LC*-circuit model perspective of the response of these textured surfaces, which identifies the engineered surface plasmon frequency with the resonant frequency of the *LC* equivalent surface impedance, by presenting the unit cell as a subwavelength resonant cavity [8]. This interpretation seems to be a powerful tool to create spoof SPPs overcoming some limitations of the corrugation geometries such as metal thickness (corrugation depth is of the order of quarter wavelength in the original proposals), as was achieved in Ref. 8, or transversal non-subwavelength confinement (a hallmark of the two-dimension hole arrays is that the cut-off frequency of the holes determines the plasma frequency, which is as well the spoof surface plasmon frequency, and thus, it is of order half wavelength. In this picture, waveguiding below diffraction of light remains undefeated since the unit cell is not truly subwavelength transversally). In Ref. 8, the "Sievenpiper mushroom" structure [9] was chosen to successfully support SPPs-like waves with high confinement on a thin substrate, but still exhibiting a narrow band response. Via these studies it became apparent that the *LC* formalism allows for the imagination of new, broader bandwidth and easier to fabricate geometries.

In the quest for a new generation of spoof SPPs geometries with improved performance in terms of bandwidth and localization, concepts developed for the design of metamaterials [10,11] may play an important role. The reason is that the atom-like unit cell structures of metamaterials, such as Split Ring Resonators (SRRs) [12] and Complementary Split Ring Resonator (CSRRs) [13], are strongly subwavelength and self-resonant in nature, which fulfils our pre-requisites for the effective medium approach, *LC* modelling and localization below the diffraction limit. To be an eligible candidate for a spoof SPP, the resonant metamaterial "particle" must be excited by p-polarized electromagnetic waves, so as to mimic SPPs (CSRR does, whereas SRR does not unless bianisotropy is present. Because of bianisotropy CSRR and SRR can be excited for certain arrangements of the particles by s- or p-polarization respectively [10]). Otherwise we would be dealing with magnetic SPPs [14] which have been suggested to provide guiding below the diffraction limit [15], but are beyond the scope of this article.

In this paper we numerically investigate the guiding of geometrically induced SPPs on both single metal-insulator (MI) interfaces and insulator-metal-insulator (IMI) multilayers (free-standing membranes) based on CSRRs using the *LC* circuit framework under PEC modelling for the metal. The latter configuration was already depicted under the Electro-Inductive waves' formalism [16, 17], but their properties were not further analysed. For comparison, and because of their similarities, classical open periodic waveguides such as a metal mesh [18, 19] are as well reviewed under this formalism, alongside the recent experimental realizations of spoof SPPs based on hole arrays [20–22] and Sievenpiper mushrooms [8]. Under the assumption that these structures are scalable within the microwave and far-infrared regime, dispersion diagrams have been normalized to the lattice period to allow for easier comparison. Furthermore, the proposed CSRRs-based MI pattern exhibits a broadband spoof SPP mode highly divergent from the light line (i.e. tight confinement), well away from the Brillouin-zone boundary. This characteristic, not shown for geometries of the literature, is desired because at the boundary the mode suffers higher propagation losses [23]. Our analysis open up new avenues for the design of spoof SPP surfaces with improved performances both in terms of confinement and bandwidth, which is of importance not only for waveguiding but also for THz sensing.

We first present the MI configuration, and the results there presented will then be extended to the IMI configuration in the next section.

2. Metal-insulator configuration: 1D array of grooves, 2D array of holes, Sievenpiper mushroom and CSRRs-based configuration

Before one can understand the complexities of Sievenpiper mushroom and CSRRs-based spoof SPPs, it may be helpful to review the classical corrugations under the transmission line formalism because of its pedagogic simplicity. The idea behind classical topologies to mimic SPPs in MI configuration relies on the transformation of the short circuit imposed by a metal

#115697 - $15.00 USD Received 13 Aug 2009; revised 11 Sep 2009; accepted 12 Sep 2009; published 24 Sep 2009

to an open circuit at the top surface plane. If we understand the cavity formed by the 1D corrugation as a transmission line terminated in a short circuit, see Fig. 1(a), we can calculate the input impedance, i.e. the surface impedance of our structure, as

$$Z_{in} = jZ_{TL}\tan(\beta h) \tag{1}$$

where Z_{TL} is the characteristic impedance of the transmission line, β the propagation constant and h the height of the cavity [24] (this analysis is valid as long as the in-plane period is much smaller than wavelength of light, $d << \lambda$). Below the pole, which occurs at $h = \lambda/4$ (assuming TEM mode as fundamental $\beta = k_0$), the input impedance is imaginary and positive and thus, the transmission line supports p-polarized waves (our geometrical induced SPP). The surface plasmon frequency corresponds in this case to the resonance associated with the divergence of Eq. (1).

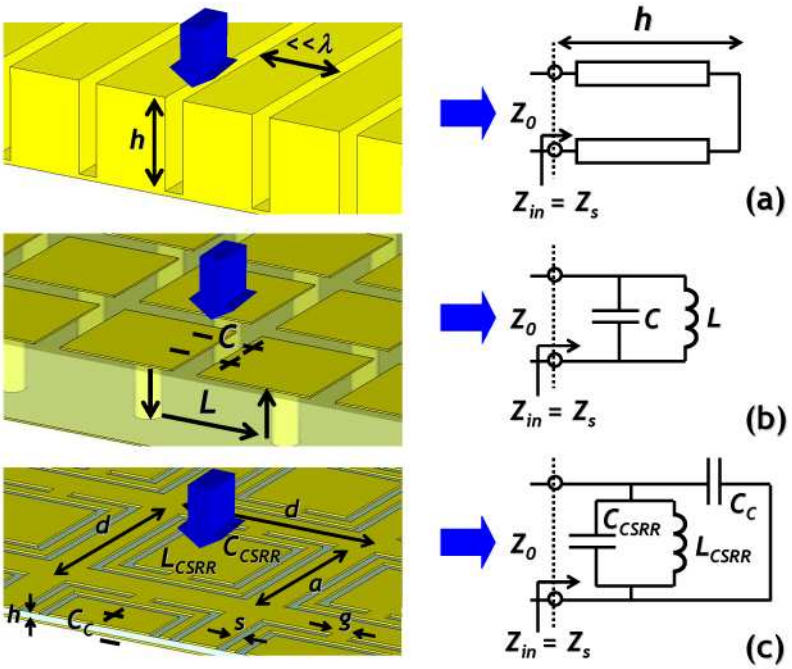

Fig. 1. Sketch (left) and circuit model (right) of the Spoof SPPs MI structures analyzed in the present work: Array of slits (a), Sievenpiper mushroom (b), and CSRRs-based metasurface (c). Blue arrows indicate the point of view of the circuit model.

The drawback of these corrugations is the thickness restriction imposed by the resonance, along with the fact that slit arrays are not appropriate for any planar guiding application because of its infiniteness along one direction. These restrictions are overcome by 2D arrays of subwavelength holes [20, 21]. However, in this case the surface impedance in engineering terms, assuming the fundamental TE_{10} mode as dominant in the cut-off region, is $Z_{in} = Z_{TL}\cdot\tanh(qh)$, where $Z_{TL} = k\cdot\eta/q$, k and η the wavenumber and intrinsic impedance of the material filling the transmission line respectively, $q = j((\pi/a)^2-k^2)^{1/2}$ and a hole size ($a << \lambda$). Unlike Eq. (1), this equation does not have any pole, resulting in a narrow band spoof SPP and (small) out-of-plane confinement caused by Brillouin-zone boundary, see Fig. 2. It is worth noting that this discussion also explains the more well-defined spoof SPP when the holes are filled with a high-index dielectric, because in this scenario, the hole may be in propagation and we come back again to Eq. (1) with $\beta = (k^2-(\pi/a)^2)^{1/2} = (\varepsilon_r\cdot k_0^2-(\pi/a)^2)^{1/2}$.

As we have seen before, the transmission line perspective is useful for an intuitive understanding of the spoof SPP response, and if we return to the fact that the spoof surface plasmon frequency is governed in 1D array of grooves by the resonance of a microwave

#115697 - $15.00 USD Received 13 Aug 2009; revised 11 Sep 2009; accepted 12 Sep 2009; published 24 Sep 2009

circuit and not by the inherent properties of the metal, we could follow two different approaches to reduce the thickness of the layer and try to increase the operating bandwidth while at the same time avoiding the undesired Brillouin-zone fold behavior of the 2D array of holes:

- Filling the cavity with a material with high dielectric constant in order to have a smaller effective wavelength. This will not be the subject of this paper.
- Find an alternative resonant circuit with inductive behavior below the resonance. This technique is addressed subsequently.

It has been Lockyear *et al.* who have recently applied the *LC* perspective by reporting geometrical induced SPP in a Sievenpiper mushroom layer [8]. By virtue of the subwavelength in-plane size of this structure, the response of the metamaterial may be characterized by an effective surface impedance. Although not strictly accurate (see description of propagation along the plane below), by simply identifying the mushroom as a parallel *LC* circuit, where *C* accounts for the electrical coupling between patches and *L* for the current from patch to patch along the vias, see Fig. 1(b), the effective surface impedance is $Z_s = j\omega L/(1-\omega^2 LC)$. Thus, for frequencies below $(LC)^{-1/2}$, the spoof surface plasmon frequency, the surface impedance is imaginary and positive, as p-polarized waves require to propagate along the surface. And at this point, a question arises: can we use the classical TM excited atom-like metamaterial CSRRs for this purpose, which is inherently self-resonant (and then the vias can be removed simplifying the fabrication)? – see Fig. 1(c). Notice that the geometry comprises a CSRR-etched top metal layer lying over a metal-backed dielectric slab.

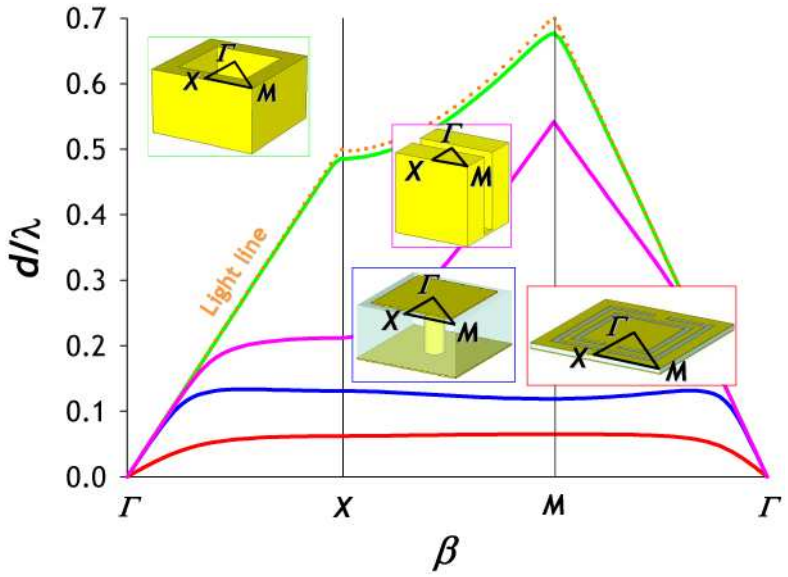

Fig. 2. Dispersion diagram normalized to the unit cell dimension *d* of the following spoof SPPs MI geometries: array of slits (pink line) and holes (green line), Sievenpiper mushroom (blue line), and CSRRs-based metasurface (red line). Light line in dotted orange line. Insets: unit cells.

From the dispersion diagrams of the topologies discussed above, presented in Fig. 2, we can draw our first conclusions since it summarizes the main characteristics of our geometrical induced SPPs. From a practical perspective important features are the operating bandwidth (frequency band within which the surface wave vector is considerably away from the light line), the out-of-plane 1/e decay length given by $l_y = \mathrm{Im}(1/k_y) = 1/(k_z^2-k_0^2)^{1/2}$ which reaches its minimum at the Brillouin-zone limit where k_z is maximum (k_0, k_y and k_z are the wavenumber in free space and along *y*- and *z*-axes, respectively. Here we have assumed without loss of generality propagation just along *z*, *Γ*-*X* in Fig. 2). The band structures have been numerically

#115697 - $15.00 USD Received 13 Aug 2009; revised 11 Sep 2009; accepted 12 Sep 2009; published 24 Sep 2009

calculated by the eigenmode solver of the Finite-Integration Frequency Domain commercial software CST Microwave Studio™. To this end, a square unit cell is taken and periodic boundary conditions are applied with specific phase shift across the cell, whereas in the top and bottom boundaries of the simulation box electric walls are employed so as to restrict our calculations to p-polarized waves. The simulated unit cells for the slit array, the array of holes and the Sievenpiper mushrooms are taken from Refs [5], [20]. and [8] respectively, whereas the unit cell of the CSRRs-based configuration is depicted in Fig. 1(c), whose parameters are: d = 8 mm, a = 6.5 mm, g = 0.8 mm, and air ring width (and metal between rings) s = 0.4 mm. Note that without loss of generality the design of this last configuration is based on a commercial microwave substrate ARLON CUCLAD 250 (dielectric constant ε_r = 2.5, height h = 0.257 mm and metallization thickness t = 0.035 mm. Note that within the rings forming the CSRR ε_r = 1) to deal with conventional materials. In all cases we have modeled the metal as perfect electric conductor which is a good approximation from the microwave to the low THz regime. Since we are normalizing the dispersion diagram to the in-plane period, the only relevant dimensions that is not represented in it is the thickness of the geometry. The values normalized to the spoof surface plasmon wavelength are $0.212\lambda_{sspp}$, $0.39\lambda_{sspp}$, $0.065\lambda_{sspp}$ and $0.003\lambda_{sspp}$ for arrays of slits, holes, mushroom and CSRRs respectively, demonstrating the thinness of the Sievenpiper and the CSRR geometry for the parameters utilized. Moreover, due to the fact that the confinement of spoof SPP decreases as the depth of the corrugation is reduced in array of slits and holes [5], these last values reveal as well the superiority of mushroom and CSRRs for thin substrates.

As discussed in Ref. 20, the array of holes mode follows the light line almost along the entire Brillouin-zone (the texture of the surface is not distinguished by the propagating wave and then, the surface behaves like a simple metallic layer) moving apart from it just at the Brillouin-zone boundary. Therefore, this slow mode is loosely confined out-of-plane and narrow band. Moreover, the unit cell is not subwavelength, it is actually more like a photonic crystal governed by diffraction/scattering phenomena in the slow wave region, and thus, it cannot be strictly characterized by an effective surface impedance. A more SPP-like response can only be achieved by filling the hole with a high-index dielectric, thereby pushing the effective geometry-induced surface plasmon frequency to lower frequencies, away from the onset of diffraction in the dispersion diagram. However, for instance, we fill the hole with ARLON CUCLAD 250, the effective spoof surface plasmon frequency lowers down only to a value of d/λ = 0.469 (without dielectric is 0.485) indicating that this dielectric is not enough to leave the photonic-crystal-like response and switch to the propagation regime of the hole.

On the other hand, the array of slits and Sievenpiper mushroom topology support a distinct spoof SPP. While their modes lie close to the air mode at low frequencies, alike the previous geometry, the frequency at which they start to bend away from it as well as the asymptotic limit are much lower than for the 2D hole arrays (namely, the spoof plasmon frequency is d/λ = 0.212 and 0.13 for slits and mushrooms respectively. When the slits are filled with ARLON CUCLAD 250, it lowers down to d/λ = 0.15, not shown in Fig. 2). This means that the unit cell is subwavelength without the need for filling with a high-index dielectric ($d = 0.212\lambda_{sspp}$ and $0.13\lambda_{sspp}$ for slits and mushrooms respectively, where λ_{sspp} is the spoof surface plasmon wavelength) and tight confinement is attainable. Nevertheless, the slits are not useful for planar guiding and the mushroom topology shows an undesired narrow band response where the mode is sensibly away from the light line as its flatness put in evidence in the dispersion diagram. It is worth noting that the slope of the latter slow mode is negative, which implies backward propagation (also known as left-handed propagation). This is readily explained from the stricter equivalent circuit model of the unit cell, shown in Fig. 3(a) from the perspective of a transmission along the surface. On the one hand, the series inductance and capacitance account for the electrical current flowing along the patch and the strong electrical coupling between patches, respectively. On the other hand, the shunt inductance and capacitance describe the current flowing along the vias and the capacitance between patches and ground. This is the transmission line of the fundamental composite right/left-handed (CRLH) circuit model [25, 26]. The pair series capacitance and shunt

#115697 - $15.00 USD Received 13 Aug 2009; revised 11 Sep 2009; accepted 12 Sep 2009; published 24 Sep 2009

inductance give support to the low-frequency backward wave, whose higher frequency is determined by the minimum of the series and shunt resonance frequencies, whereas the combination of the series inductance and shunt capacitance leads to the conventional right-handed propagation above the maximum of the series and shunt resonance frequencies (mode not illustrated in Fig. 2). However, this picture is not so simple because this is an open waveguide, and then, the part of the LH mode that lies within the cone of light (where $k < k_0$) couples with the TM RH air mode, leading to a mixed LH-RH fundamental mode [26].

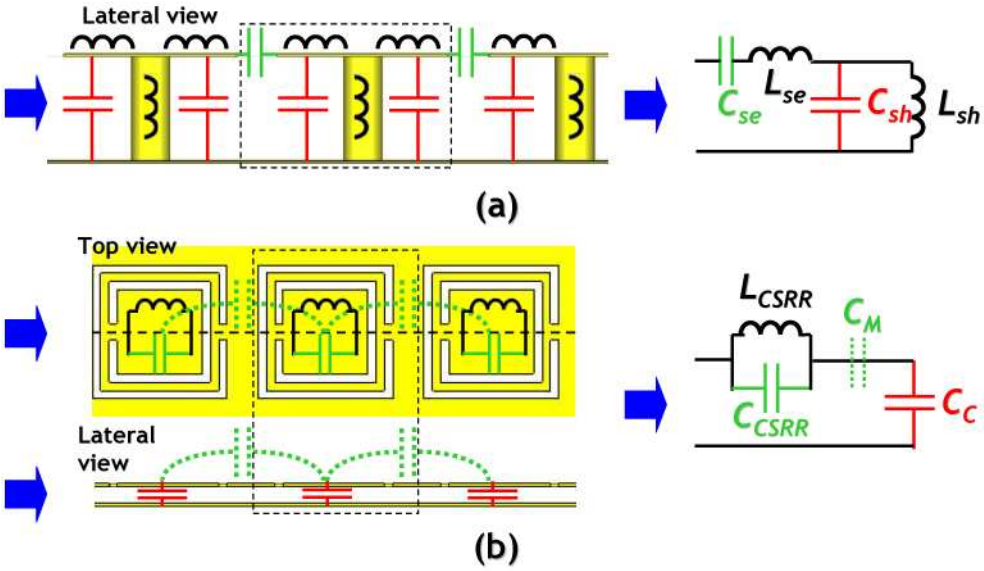

Fig. 3. Equivalent circuit model for (a) Sievenpiper mushrooms and (b) CSRRs-based SPP. To understand the origin of the different components, they have been superimposed onto the sketches of the geometries.

Finally, the proposed CSRRs-induced SPP gives a different scenario. The slow wave moves away from the light line as soon as it leaves DC (broadband response) and its spoof surface plasmon frequency is the lowest of the three studied configurations (thus, l_y is smaller than for the preceding configurations, that is, tight confinement is achieved). In this case the slope of the mode is always positive. The slow and forward propagation character of this case can be explained again by a simple equivalent circuit model, see Fig. 3(b). Assuming that the coupling between CSRRs is negligible, the equivalent circuit model of the CSRRs is a *LC* tank [10] which replaces the series branch of the previous transmission line, whereas the shunt inductance is no longer present because of the absence of vias. The resultant transmission line supports forward waves, but no longer backward waves. The introduction of the potential electrical coupling between adjacent CSRRs in series with the *LC* tank in the equivalent circuit modifies slightly the frequency response, but it does not affect the handedness of the propagation.

The operating principle of the CSRRs can be as well explained from the perspective of surface impedances, as we did at the beginning of this section for others topologies, by using the same equivalent circuit model. However, in this case the input port (indicated by blue arrows) changes its position as Fig. 1(c) depicts. This representation of the metasurface in free space by a four-terminal network is possible only in the long wavelength regime, where no propagating diffraction orders exits. Let us reconstruct the circuit (unit cell) from the point of view of an electromagnetic wave coming into contact with our surface to understand the reason of each component. First, an impinging wave encounters the impedance associated to the CSRR, the *LC* tank, and afterwards a short circuit ended transmission line whose impedance seen just after the CSRR is defined by Eq. (1), and thus, has an inductive character. Then, the surface impedance can be expressed as a parallel connection of the CSRR

#115697 - $15.00 USD Received 13 Aug 2009; revised 11 Sep 2009; accepted 12 Sep 2009; published 24 Sep 2009

impedance and the surface impedance of the grounded dielectric slab. However, the length of our cavity is so small in terms of the spoof surface plasmon wavelength that it redraws the picture of this last section. Firstly, as a result of the negligible length, the short can be placed as if it were just after the CSRR. And secondly, at resonance, the CSRR induces a strong electric dipole perpendicular to the surface [13] which, alongside the short distance between metallic layers, may introduce a strong capacitance C_c, arriving at the circuit model of Fig. 3(b). By simple inspection of the circuit of Fig. 1(c), the spoof surface plasmon frequency is $(L_{CSRR}\cdot(C_{CSRR}+C_c))^{-1/2}$. If the second assumption brought into play to account for C_C is valid, the spoof surface plasmon frequency should be sensitive to the distance between metallic layers since $C_c = \varepsilon_r \cdot d^2/h$. In consequence, the longer h (smaller ε_r), the higher the spoof surface plasmon frequency. This has been checked by changing both ε_r and h, see Fig. 4, where smaller h or greater ε_r produces a lower saturation frequency in agreement with our hypothesis. Needless to say, if we start increasing the distance between metallic layers, the transmission line modeled by Eq. (1) should be included in the circuit model.

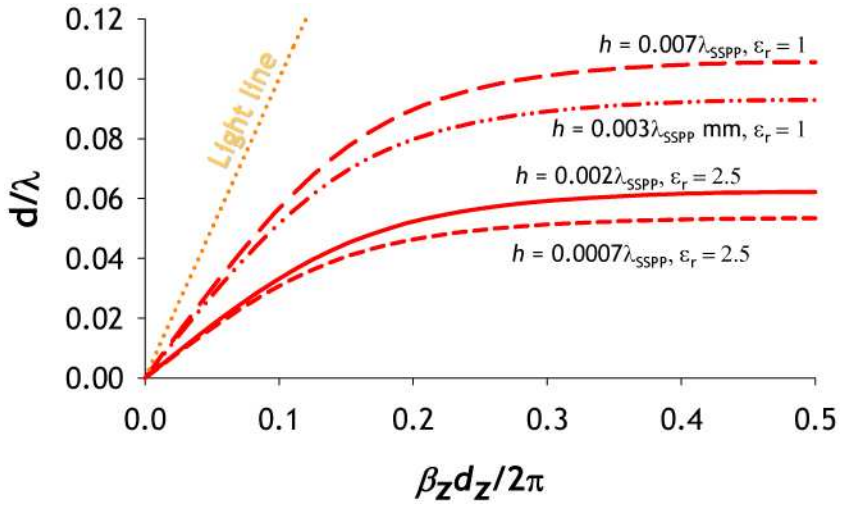

Fig. 4. Dispersion diagram of the CSRRs-induced spoof SPPs for different values of height and permittivity of the dielectric slab.

After some algebra, we can also derive the resonance for the circuit with the mutual coupling (additional capacitance C_M plotted in Fig. 3(b) by green dotted lines) between adjacent CSRRs, $\omega = ((L_{CSRR}\cdot(C_{CSRR}\cdot C_M+C_C\cdot(C_{CSRR}+C_M))/(C_C+C_M))^{-1/2}$. Nevertheless, the only intuitive conclusion that can be extracted from this equation is that there is still a resonant frequency which mimics the surface plasmon frequency regardless of the inclusion of the mutual coupling.

To further investigate the prospects of spoof SPP in the CSRRs geometry, we plot in the yz-cutting plane at $x = 0$ (middle plane of our unit cell) the electric field of the eigenstate supported by our unit cell at the spoof surface plasmon frequency, see Fig. 5(a). Arrows point in the direction of the E-field, whereas its color and size illustrate the magnitude of the E-field. The gray scale background illustrates the magnitude of the magnetic field H_x. In the top air-metal interface the electric field distribution indeed resembles that of SPPs. On the other hand, the field no longer resembles a SPP mode in the space between the metal layers because of the strong coupling, but this is an unavoidable feature in such ultrathin geometry. Moreover, we complete the study by representing in Fig. 5 $|E_y|$ and $|E_z|$ for a chain of 25 unit cells (a planar waveguide with pitch d = 8 mm and total thickness $h+2t$ = 0.327 mm, where t is the metal thickness) at the same yz-cutting plane along with the electric energy density close to the spoof surface plasmon frequency (f = 2.3 GHz $\approx 0.99 f_{SSPP}$, where f_{SSPP} is the effective spoof SPP frequency), see Figs. 5(b), 5(c) and 5(d) respectively. The total length of the waveguide is 200 mm $\approx 1.53\lambda$. To do so, the structure is excited by a monopole placed at

#115697 - $15.00 USD Received 13 Aug 2009; revised 11 Sep 2009; accepted 12 Sep 2009; published 24 Sep 2009

the beginning of the structure, using in this case the time domain transient solver of CST Microwave Studio™ for the simulation. As it is expected from a spoof SPP, exponential decay is observed along *y*, exhibiting subwavelength out-of-plane confinement: for instance, the 1/e decay length from the surface is 0.3 mm ≈0.0023λ and 0.34 mm ≈0.0026λ at the center of an arbitrary CSRR and in the middle between two CSRRs respectively. Notice that these figures of merit take into account the spoof SPP along with the free space propagating wave, although the latter is negligible with respect the spoof SPP as Fig. 5(b) highlights. Furthermore, the electric energy density is confined to the dimensions of the CSRR (6.5 mm ≈0.05λ), and thus, this geometry displays as well subwavelength in-plane confinement.

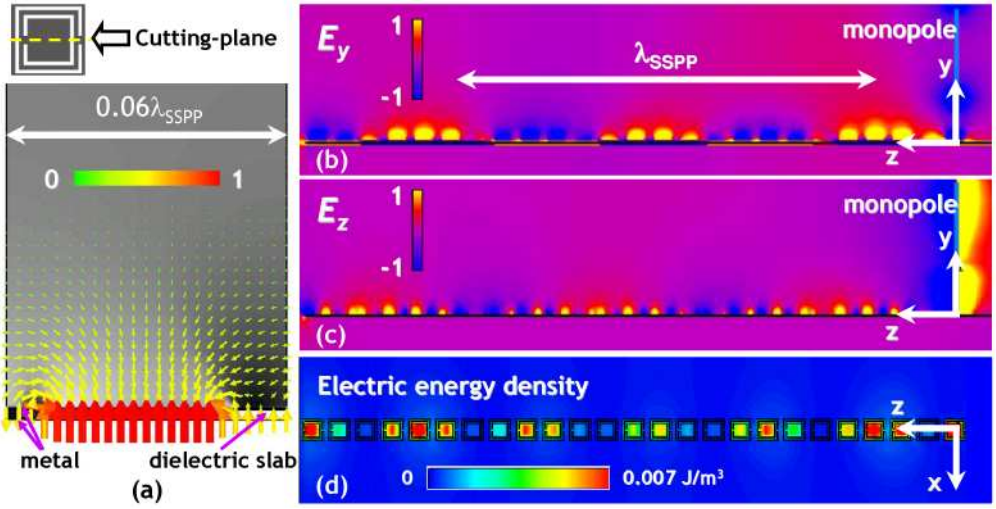

Fig. 5. (a) Electric field, arrows, and $|H_x|$ background gray scale within the unit cell (fundamental eigenmode); Cross-sectional view at the middle plane of a chain of 25 unit cells ($1.6\lambda_{SSPP}$) of $|E_y|$ (b), and $|E_z|$ (c) in arbitrary units; (d) Electric energy density along the planar waveguide.

3. Insulator-metal-insulator configuration: metal mesh, array of subwavelength holes and array of CSRRs

In the 1960s and 70s, Ulrich *et al.* studied intensively the properties of the wire mesh in the far infrared (within what we call now THz region) as an open periodic waveguide [18, 19] to correlate them with the results of the wire mesh acting as a screen [27]. In the analysis of the waves supported by the thin mesh, they observed that the dispersion curve of the Sommerfeld-Zenneck wave was modified by the periodicity (because of Bragg reflection at the Brillouin-zone boundary) in such a way that a slow wave (trapped waves according to their nomenclature) was achieved for the first mode, see Fig. 6. From the point of view of SPP this is nothing but the first and simplest attempt to mimic SPP in an IMI scenario [3, 5]. Thus, despite the achievement of some out-of-plane confinement of the Sommerfeld-Zenneck wave, the response is narrow band and lossy because of scattering at the Brillouin-zone border.

In order to decrease the out-of-plane 1/e decay length l_y, that is, increase the out-of-plane confinement which was still small on metal meshes, the strategy followed in Ref. 22 was to push down the saturation frequency – consequently increasing the denominator of l_y – by approaching to the problem according to Ref. 3. The permittivity of a holey metal exhibits an effective plasma frequency defined by the cut-off frequency and thus, the condition for the existence of SPPs $\varepsilon_{eff\_metal} < -\varepsilon_{insulator} < 0$ is attainable at any desired frequency range [3]. Moreover, with the purpose of further increasing the denominator of l_y (at the Brillouin-zone boundary, $l_y = 1/((\pi/d_z)^2-(\omega/c)^2)^{1/2}$), rectangular holes were designed (blue inset of Fig. 6) to allow reducing the lattice constant along the direction of propagation *z*, d_z, *Γ-X* in Fig. 6.

#115697 - $15.00 USD Received 13 Aug 2009; revised 11 Sep 2009; accepted 12 Sep 2009; published 24 Sep 2009

We now investigate whether the CSRR-approach based on inducing the surface plasmon frequency is still valid for IMI topology. Unlike the previous IM proposal, the geometry now just comprises a CSRR-etched metal layer, without the metal-backed dielectric slab. Again, it seems to be no limitations, as the dispersion diagram of coplanar-CSRRs arrangement (without the bottom metal layer of the previous MI topology) shows, see red line in Fig. 6. Unlike the metal mesh or the array of subwavelength holes, the saturation frequency of arrays of CSRRs is not governed by the Bragg reflection or a cut-off frequency, but by the quasi-static resonance of the CSRR, see Fig. 6. This fact has two strong consequences for IMI configurations, already highlighted in preceding section for MI: (1) potential high out-of-plane confinement if the quasi-static frequency is pushed down, and (2) the effective medium approach is applicable because of the subwavelength nature of the particle.

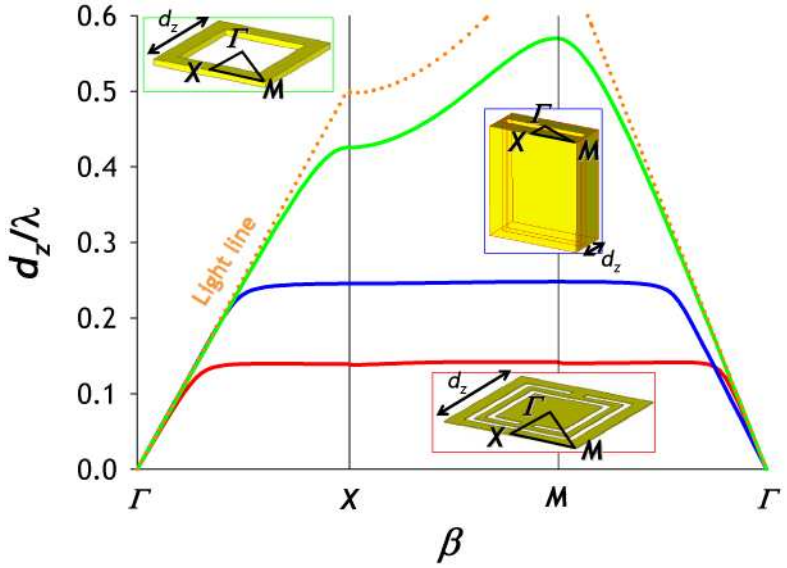

Fig. 6. Dispersion diagram of the following spoof SPPs IMI geometries: metallic mesh (green line), rectangular holes (blue line), and CSRRs-based metasurface (red line). Light line in dotted orange line. Notice that in the case of rectangular holes we are dealing with two different in-plane lattice constants and the normalization is done to the shortest one. That is why blue curve does not follow the light line in *M*-*Γ* zone for low frequencies. Insets are not to scale to each other. Only fundamental modes are represented.

Another feature that reveals Fig. 6 is that, as it happens to Sievenpiper mushrooms in the MI configuration, the fundamental mode is a mixture of LH-RH behavior. The forward propagation comes as a result of the coupling to the air mode, whereas the backward is explained in terms of Electro-Inductive waves' formalism [16, 17]. Backward propagation of electroinductive waves supported by a chain of stacked CSRR metasurfaces has been experimentally demonstrated in [28]. The parallel resonant *LC* tank formed by the CSRR (note that now the surrounding metal, that is, the metal layer itself, plays the role of the ground plane [13, 16, 28]) along with the series capacitance that accounts for the electrical coupling between adjacent resonators supports backward propagation, see Fig. 7. This circuit model is a simplified version of the CRLH transmission line of Fig. 3(a) where the series inductance has been removed. It is worth noting that this chain of CSRRs resembles straightforwardly the coupling between closely spaced metal nanoparticles [29]. And thus, the simplicity with which experiments on Electro-Inductive waves can be carried out may serve as an excellent platform for demonstrating ideas emerging in the field of nanoparticles. However, this is not addressed in this work.

Unlike the MI configuration, the arrangement of CSRRs exhibits now a narrowband behavior, because its frequency response is only governed by the narrow resonance of the

#115697 - $15.00 USD Received 13 Aug 2009; revised 11 Sep 2009; accepted 12 Sep 2009; published 24 Sep 2009

CSRRs. On the contrary, in the MI geometry, the frequency response may be dictated by the CSRRs alongside the parallel plate waveguide formed due to the two metal layers. This transmission line is known to supports propagating waves which may explain the broadband spoof of the MI configuration.

If we want to derive the response of the surface impedance in order to find the spoof surface plasmon frequency, we just have to remove C_c in the circuit model of Fig. 1(c) and replace the right-hand side by the infinite free space transmission line, see Fig. 7(a). It is straightforward to see that, whether including the mutual coupling between adjacent resonators C_M or not, the spoof surface plasmon frequency is $(L_{CSRR} \cdot C_{CSRR})^{-1/2}$. This agrees well with the fact that the dispersion diagram of the IMI topology, Fig. 6, predicts a higher saturation frequency than the MI geometry, Fig. 2, because of the absence of C_c. Needless to say, the circuit model is valid for frequencies below the onset of the higher diffraction order.

To reinforce the *LC* perspective of this paper in conjunction to surface impedances, Fig. 7(b) presents the normalized (to free space impedance) surface impedance of a CSRRs metasurface obtained by the S-parameters retrieval method [30]. At 0.141 the surface impedance exhibits a resonance associated to the resonance of the *LC* tank of Fig. 7. Below this resonant frequency, the surface impedance has an inductive behavior and may support spoof SPP (see Fig. 6), whereas above this frequency, it turns to be mainly resistive.

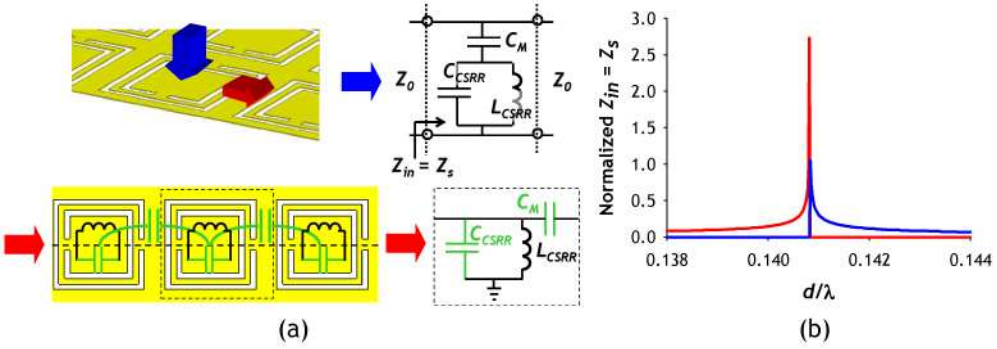

Fig. 7. (a) Equivalent circuit model for CSRRs-based SPP from surface impedance perspective (top) and transmission line along the surface (bottom). (b) Normalized impedance of a metasurface composed of CSRR: Real part (blue line) and imaginary part (red line).

As we did in the previous section, we plot in the *yz*-cutting plane at $x = 0$ (middle plane of our unit cell) the electric field of the eigenstate supported by our unit cell at the spoof surface plasmon frequency, see Fig. 8(a), with the same meaning for arrows and color as before. The distribution of the electromagnetic fields resembles in this case the short-range SPP (also called even mode). Figures 8(b) and 8(c) display the electric field $|E_y|$ and $|E_z|$ respectively in the aforementioned *yz*-cutting plane in a chain of 25 CSRRs forming a planar IMI spoof SPP waveguide (pitch $d = 8$ mm $\approx 0.14\lambda$, lateral size of the exterior air ring $a = 6.5$ mm $\approx 0.11\lambda$ and total length of the chain 200 mm $\approx 3.5\lambda$. Note that the total thickness of the topology corresponds to the metal thickness $t = 0.035$ mm $= 0.0006\lambda$) at $f = 5.2$ GHz $\approx f_{SSPP}$. Similar conclusion about these field representations alongside the electric energy density, Fig. 8(c) – see as well Ref. 16 –, drawn for the MI geometry can be brought about here to claim again subwavelength guiding and tight confinement in this IMI geometry. However, we cannot accurately determine the 1/e decay for out-of-plane confinement as before, because the free space grazing wave intensity is in this case of the same order of the spoof SPP. It should be mentioned that the electric energy density has much lower values than in the MI case because the monopole is not as well-matched (its reflection coefficient does not reach reasonable low values) to the chain as in the MI geometry. Nevertheless, subwavelength confinement in- and out-of-plane should be readily achievable also in this geometry.

#115697 - $15.00 USD Received 13 Aug 2009; revised 11 Sep 2009; accepted 12 Sep 2009; published 24 Sep 2009

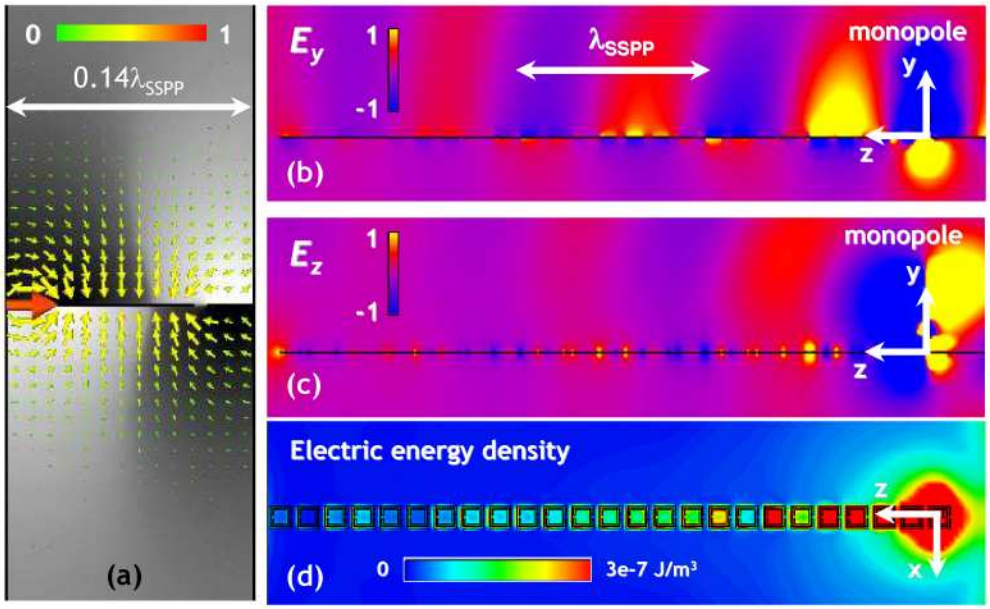

Fig. 8. (a) Electric field, arrows, and $|H_x|$ background gray scale within the unit cell (fundamental eigenmode); Cross-sectional view at the middle plane of a chain of 25 unit cells ($3.5\lambda_{SSPP}$) of $|E_y|$ (b), and $|E_z|$ (c) in arbitrary units; (d) Electric energy density along the planar waveguide.

4. Conclusion

A review of different spoof surface plasmon polaritons in both metal-insulator and insulator-metal-insulator topologies available in the literature is presented, alongside a new proposal based on complementary split ring resonators. The drawbacks of classical spoof SPPs such as small out- and in-plane confinement and narrow band response are identified in each topology and overcome by the CSRRs-based geometry. Moreover, the reported CSRRs-based geometries are at least one order of magnitude thinner than those found in the literature. A planar subwavelength waveguide based on the new class of spoof SPPs is numerically analyzed, showing high out- and in-plane confinement, as expected from the dispersion diagram and the subwavelength unit cell dimensions. The numerical analysis is supported by simple circuit models under a transmission line perspective. The simplicity of the approach and its easy manufacture by printed circuit board techniques make these CSRRs induced spoof SPPs a promising candidate for surface waveguiding in the microwave and THz regime of the spectrum.

Acknowledgments

The authors acknowledge the fruitful discussion with Dr. A.I. Fernández-Domínguez. This work has been supported by Spanish Government and E.U. FEDER funds under contracts Consolider "Engineering Metamaterials" CSD2008-00066 and TEC2008-06871-C02-01, and by the US Air Force Office of Scientific Research (AFOSR Award FA 9550-07-1-0441). M. Navarro-Cía also acknowledges financial support from grant FPI of MICINN (project no. TEC2005-06923-C03-01).

#115697 - $15.00 USD Received 13 Aug 2009; revised 11 Sep 2009; accepted 12 Sep 2009; published 24 Sep 2009